PAPER

Selective delivery of an anticancer drug with aptamer-functionalized liposomes to breast cancer cells *in vitro* and *in vivo*†

Hang Xing,‡[ad] Li Tang,‡[b] Xujuan Yang,‡[c] Kevin Hwang,[a] Wendan Wang,[c] Qian Yin,[b] Ngo Yin Wong,[b] Lawrence W. Dobrucki,[d] Norio Yasui,[a] John A. Katzenellenbogen,[a] William G. Helferich,*[c] Jianjun Cheng*[b] and Yi Lu*[abd]

Selective targeting of cancer cells is a critical step in cancer diagnosis and therapy. To address this need, DNA aptamers have attracted significant attention as possible targeting ligands. However, while their use in targeting cancer cells *in vitro* has been reported, their effectiveness has rarely been established *in vivo*. Here we report the development of a liposomal drug delivery system for targeted anticancer chemotherapy. Liposomes were prepared containing doxorubicin as a payload, and functionalized with AS1411, a DNA aptamer with strong binding affinity for nucleolin. AS1411 aptamer-functionalized liposomes increased cellular internalization and cytotoxicity to MCF-7 breast cancer cells as compared to non-targeting liposomes. Furthermore, targeted liposomal doxorubicin improved antitumor efficacy against xenograft MCF-7 breast tumors in athymic nude mice, attributable to their enhanced tumor tissue penetration. This study suggests that AS1411 aptamer-functionalized liposomes can recognize nucleolin overexpressed on MCF-7 cell surface, and therefore enable drug delivery with high specificity.

Introduction

A major challenge in nanomedicine for cancer diagnosis and therapy is the delivery of imaging agents or anticancer drugs specifically and efficiently.[1–5] To achieve this goal, the use of targeting or recognition motifs for active targeting is considered one of the most promising approaches.[6,7] Small molecules, targeting peptides, as well as antibodies have been widely reported as targeting agents.[8–10] However, when incorporated with nano-materials, the properties of the resulting constructs are often dictated more by the material used rather than the targeting agent,[11,12] and consequently developing targeted nanomedicines capable of potential clinical use is still challenging.[13,14]

To meet these challenges, DNA aptamers have been investigated as a new class of targeting agent.[15–17] Aptamers are single-stranded oligonucleotides that can bind to target molecules with excellent specificity and affinity.[18–22] In comparison to antibodies, which suffer from problems with instability and immunogenicity, DNA aptamers are stable in harsh environments and have been demonstrated to be non-immunogenic.[23] They are easier to prepare and to conjugate to nanomedicine-based platforms.[24,25] In addition, the targeting functionality of DNA aptamers can be inhibited by complementary DNA sequences, which can thus function as a specific antidote to prevent overdosage in drug delivery.[26] Moreover, in comparison with various previously reported RNA aptamers, DNA aptamers showed reduced susceptibility to biodegradation, which makes them more favorable for clinical applications.

Liposomes are one of the most successful nanomedicine delivery platforms, and have been used to deliver a wide variety of small molecules, genes, imaging agents, and even nanoparticles.[27,28] Compared with other delivery systems, liposomes offer superior biocompatibility, biodegradability, reduced toxicity and improved control over size and surface functionality.[29] Since liposomes have previously been approved by the United States Food and Drug Administration (FDA) for a number of clinical therapies, starting from this scaffold and incorporating DNA aptamers to incorporate targeting functionality should potentially facilitate the translation to clinical practice. Despite this promise, few studies of DNA aptamer–nanomedicine constructs have shown successful efficacy *in vivo*, even though the use of DNA aptamers for targeted drug

[a]*Department of Chemistry, University of Illinois at Urbana–Champaign, Urbana, Illinois 61801, USA. E-mail: yi-lu@illinois.edu; Tel: +1-217-333-2619*

[b]*Department of Materials Science and Engineering, University of Illinois at Urbana–Champaign, Urbana, Illinois 61801, USA. E-mail: jianjunc@illinois.edu; Tel: +1-217-244-3924*

[c]*Department of Food Science and Human Nutrition, University of Illinois at Urbana–Champaign, Urbana, Illinois 61801, USA. E-mail: helferic@illinois.edu; Tel: +1-217-244-5414*

[d]*Beckman Institute for Advanced Science and Technology, University of Illinois at Urbana–Champaign, Urbana, Illinois 61801, USA. Tel: +1-217-244-5023*

† Electronic supplementary information (ESI) available. See DOI: 10.1039/c3tb20412j

‡ These authors contributed equally to this work.

Paper | Journal of Materials Chemistry B

delivery *in vitro* has been reported.[26] Demonstrating the efficacy both *in vitro* and *in vivo* is important to advance nanomedicine.
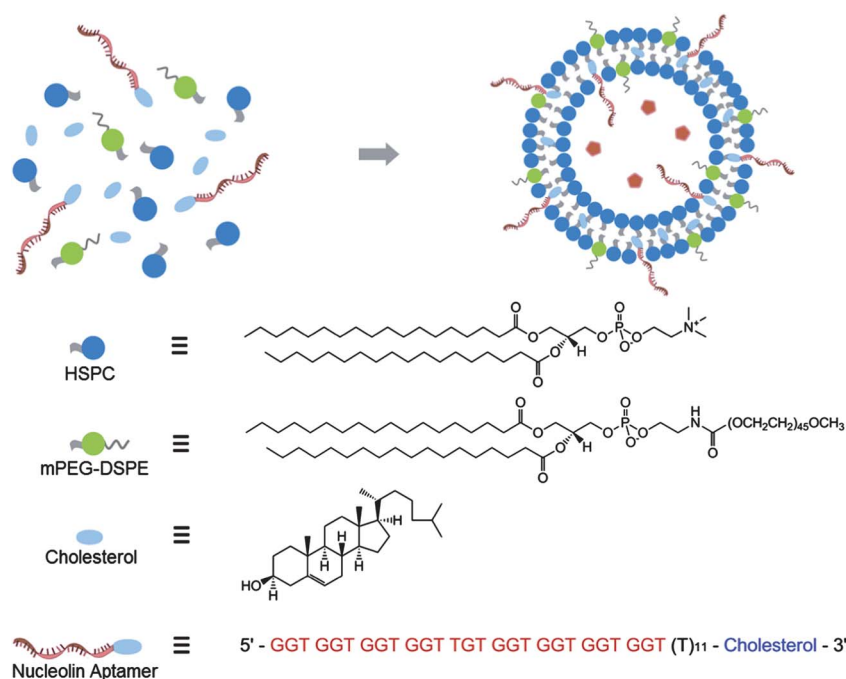
In order to investigate this issue, we prepared a nanoscale liposome modified with a 26-mer guanosine-rich DNA aptamer AS1411. AS141 has strong binding affinity to nucleolin (NCL), a *bcl2* mRNA-stabilizing protein overexpressed on the plasma membrane of many types of cancer cells, including leukemia and breast cancers.[30–33] AS1411 has been shown to be remarkably stable against nuclease degradation in serum, which is attributed to the formation of the G-quartet structure.[34] Further pharmacokinetic studies have shown enhanced stability of AS1411 in blood *in vivo*, which overcomes one of the major limitations reported for potential aptamer use in clinical practice.[35] In previous work, we have demonstrated that the AS1411 DNA aptamer (Apt) facilitated the cellular uptake of cisplatin-containing liposomes and showed higher cytotoxicity to MCF-7 cells than the same liposome system without the aptamer or with a non-aptameric DNA strand (Ctrl).[26] While these *in vitro* results are promising, it is important to demonstrate the efficacy of the approach *in vivo* for future clinical applications.

In this study, we report the preparation of AS1411 aptamer-functionalized liposomes containing an anticancer drug, doxorubicin (Dox). The targeted liposomal doxorubicin (Apt-Dox-Lip) showed selective internalization and enhanced cytotoxicity to MCF-7 breast cancer cells. Athymic nude mice bearing xenograft MCF-7 tumors treated with intratumorally injected Apt-Dox-Lip exhibited an earlier onset of tumor inhibition and improved anticancer efficacy when compared with non-aptameric DNA modified congeners, which is attributable to enhanced tumor penetration and cellular internalization.

Results and discussion

Preparation and characterization of DNA-functionalized liposomes

Fig. 1 illustrates the basic design and formulation of aptamer-functionalized liposomes containing different cargos. The sequence of the NCL aptamer used is 5′-GGT GGT GGT GGT TGT GGT GGT GGT GGT TTT TTT TTT TT-Cholesterol-3′. The poly-T region in the above sequence serves as a spacer to separate the aptamer recognition sequence from the hydrophobic cholesterol end. A non-aptameric DNA sequence 5′-GAG AAC CTG AGT CAG TAT TGC GGA GAT TTT TTT TT-Cholesterol-3′ was used as a control. Doxorubicin hydrochloride was chosen as the anticancer agent. Aiming at potential clinical applications of DNA aptamer-modified liposomes, a well-established liposome formulation was used as model system for DNA aptamer modification. The liposomes were formulated from HSPC, cholesterol, and mPEG2000-DSPE at a molar ratio of 2 : 1 : 0.16.[36] The aptamer-modified liposome based on this formulation structurally resembles Doxil®, an FDA-approved, doxorubicin-containing liposome, except that the latter has no targeting ligand incorporated.[37] This HSPC/Cholesterol/DSPE-PEG formulation has been intensively studied for many years and was reported to be effective for *in vivo* applications. The combination of HSPC and DSPE possesses a relatively high transition temperature at 48 °C, providing liposomes with high rigidity and low permeability at 37 °C.[36] Free cholesterol molecules serve as hydrophobic anchors to increase the hydrophobic–hydrophobic interactions in lipids bilayer as well as the rigidity and stability of liposomes.[36] The inert, hydrophilic PEG modification reduces the nonspecific uptake of liposomes.[38] The formulation of liposomes provides an excellent system with

Fig. 1 Schematic illustration of the NCL Aptamer-conjugated liposome with encapsulated cargo. HSPC, cholesterol, and mPEG2000-DSPE were mixed in a 2 : 1 : 0.16 molar ratio. Cholesterol-modified DNA strands were immobilized onto the surface of liposome by intercalating the 3′ cholesterol modification into the lipid bilayer.
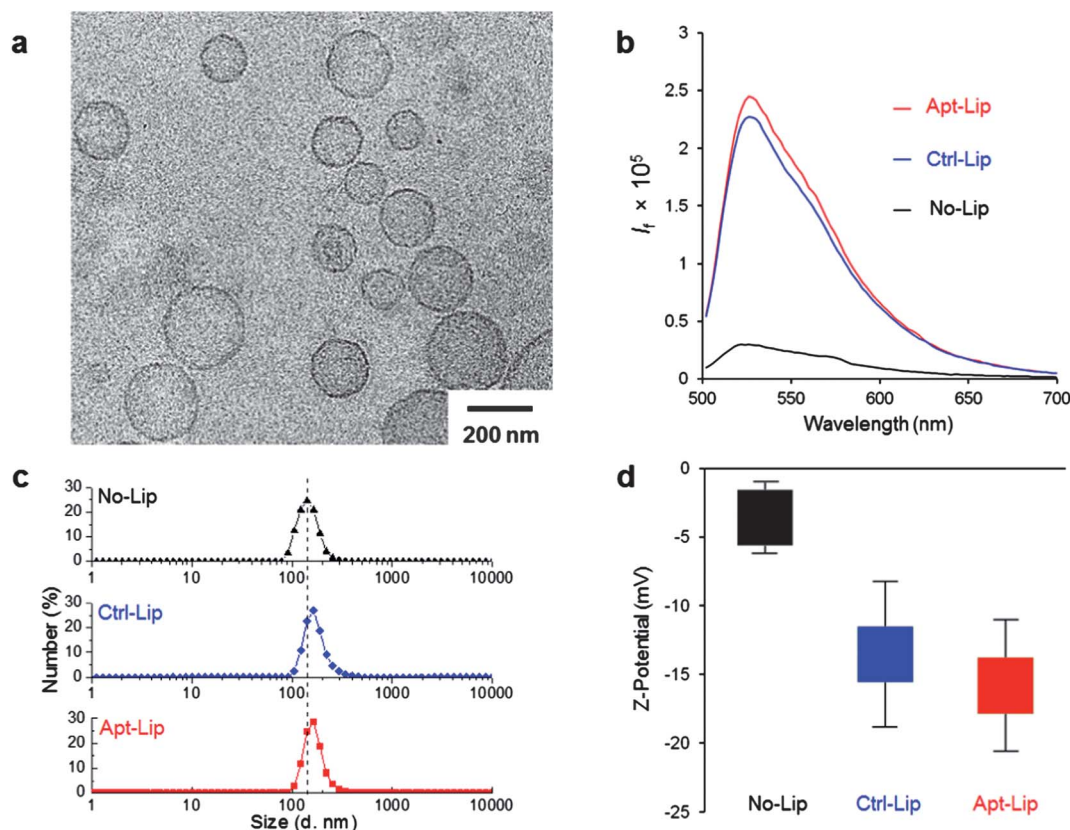
Nucleolin Aptamer ≡ 5′ - GGT GGT GGT GGT TGT GGT GGT GGT GGT (T)₁₁ - Cholesterol - 3′

long-term stability suitable for the *in vivo* study of aptamer-directed targeted drug delivery.

The NCL aptamer-functionalized liposomes of ∼200 nm in diameter were prepared according to a previously published protocol, using polycarbonate membrane supported extruders.[26] In a typical experiment, the overall lipid concentration was controlled at ∼8 mg mL^{-1} in the presence of 12 μM cholesterol–DNA in a preparation buffer (pH 7.4) containing 25 mM HEPES, 150 mM NaCl, 5 mM KCl, 1 mM MgCl$_2$, and 1 mM CaCl$_2$. The prepared Dox-containing Apt-liposomes can be easily concentrated *via* centrifugation (Fig. S2a†). Under a fluorescence microscope, a solution of dye-containing liposomes was observed as separate bright dots, confirming the formation of lipid vesicles (Fig. S2b†). To further elucidate the structure and morphology of aptamer-modified liposomes, Cryo-EM experiments were performed. As shown in Fig. 2a, the liposomes appeared spherical with a lipid bilayer membrane thickness of several nanometers. The average size is around ∼200 nm, which agrees well with the pore size of the polycarbonate membrane used in preparation.

To demonstrate the functionalization of liposomes with the DNA aptamer and to achieve a quantitative measure of the DNA density on each liposome, we used a commercially available green-fluorescent stain, OliGreen® ssDNA reagent, to measure the DNA concentration. Prior to the staining process, Triton-X and heat treatment (80 °C) was used to break the lipid vesicles and release DNA strands. The ruptured liposome samples were incubated with the OliGreen® reagent for 10 min and excited at 480 nm. As shown in Fig. 2b, liposomes without the DNA aptamer functionalization showed only a low level of background fluorescence. After attachment of DNA aptamer, Apt-Lip and Ctrl-Lip samples exhibited a strong fluorescence emission peak at 520 nm after staining, demonstrating the presence of ssDNA. Quantitative measurement of DNA concentration in the liposome samples was achieved using a calibration curve generated from a series of standard DNA solutions (Fig. S1†). The DNA aptamer concentration of Apt-Lip sample was calculated to be 9.7 μM, with a corresponding conjugation efficiency of ∼34.6%. The DNA density per liposome was estimated to be ∼1.1 nmol DNA adsorbed on 1.0 mg of lipids.

The DNA-functionalized liposomes were further characterized by Dynamic Light Scattering (DLS) and ξ-potential measurements. Liposomes without the DNA aptamer functionalization showed an average hydrodynamic diameter of 190 ± 16 nm, which is consistent with the Cryo-EM images. After DNA functionalization, an average hydrodynamic

Fig. 2 (a) Cryo-EM micrographs of Apt-Dox-Lip samples. The average liposome size is around 200 nm. (b) Fluorescent spectra of OliGreen® ssDNA reagent stained Apt-Lip, Ctrl-Lip, and No-Lip samples. Sample solution was treated with Triton-X and heated at 80 °C for 20 minutes to break the lipid bilayer and release DNA strands before staining. λ_{ex} = 480 nm. λ_{em} = 520 nm. (c) Representative DLS and (d) ξ-potential results of different liposome samples with NCL-aptamer (Apt-Lip, red), control DNA (Ctrl-Lip, blue), and without any DNA (No-Lip, black). The reported hydrodiameter and ξ-potential of liposome samples were calculated from the algebraic average of twenty measurements. Bars represent standard deviation.

diameter of 210 ± 20 nm was observed for both aptamer and control DNA-modified liposomes (Fig. 2c). In order to further understand the effect of DNA modification on the surface of liposomes, we measured the ξ-potential of different liposome samples. In a 5 mM HEPES buffer (pH 7.4) containing 10 mM NaCl, liposomes without the DNA aptamer functionalization displayed a ξ-potential of -4 ± 2 mV, which is consistent with previously reported values for liposomes with this composition.[25] After conjugation with the DNA strands, the ξ-potential of control and aptamer DNA-modified liposome samples decreased to approximately -15 ± 5 mV, further indicating the attachment of negatively charged DNA strands on the surface of the liposomes (Fig. 2d).

Since the *in vivo* biological microenvironment is significantly different from the liposome preparation buffer, it is critical to evaluate the stability of the liposomes under physiological conditions before proceeding to cellular and animal studies. In order to evaluate the stability of the DNA-modified liposomes, we monitored the fluorescence intensity of NCL aptamer-modified, uranin-containing liposome samples (Apt-Urn-Lip) after incubation at 37 °C in 50% human serum over a period of 24 hours (Fig. 3a). Fully ruptured Apt-Urn-Lip samples were used as positive control group to illustrate the fluorescent intensity after complete release of uranin (black line). As shown in Fig. 3b, after 24 hours at 37 °C in 50% human serum, less than ~10% of the maximum possible enhancement of fluorescence intensity was observed, suggesting only minimal decomposition of the liposome samples and minimal leakage of encapsulated uranin. Similar release profile was observed for doxorubicin-loaded liposome samples (Fig. S3†). These results indicate that the aptamer modified liposome samples are highly stable in 50% human serum with well-preserved fluorescent properties.

Towards the goal of achieving an enhanced anticancer therapy *in vivo*, it is also critical to control the drug loading in order to provide sufficient anticancer agent in the aptamer–liposome system. The DNA–lipid mixture was incubated with ~25 mg mL^{-1} Dox solution to achieve high Dox loading. The fluorescence of the DNA-Dox-Lip sample was measured by excitation at 480 nm before and after heat treatment (Fig. S4a†). According to a standard curve of free doxorubicin, the
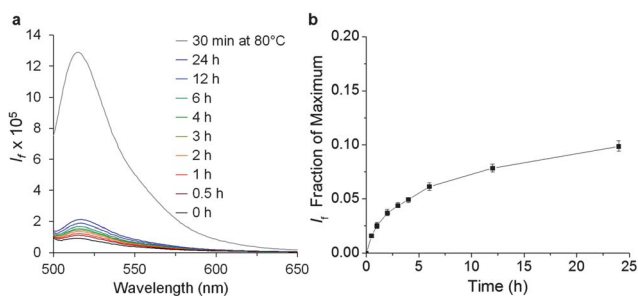
equivalent Dox concentration of a typical Apt-Dox-Lip sample was calculated to be 0.92 mg mL^{-1} based on fluorescence emission intensity of fully decomposed liposomes at 592 nm (Fig. S4b and S4c†). The drug-to-lipid ratio of the Apt-Dox-Lip sample was estimated to be 0.097 (w/w), which is comparable to the 0.125 (w/w) drug-to-lipid ratio of Doxil®,[39] suggesting a sufficient drug loading capacity for *in vivo* study.

In vitro targeting capability of aptamer-functionalized liposomes

To assess the targeting capability of aptamer-functionalized liposomes, uranin-loaded liposomes that were modified with control DNA (Ctrl-Urn-Lip, 50 μM lipid equivalent) or NCL-Apt (Apt-Urn-Lip, 50 μM lipid equivalent) were incubated with MCF-7 cells separately, and the fluorescence of the treated cells was analyzed by flow cytometry (Fig. 4a and Table S1†). In order to compare their binding affinity with MCF-7 cells, a low sample concentration (50 μM lipid equivalent) and a 4 h incubation time was used. The results showed a 6.6-fold increase in mean fluorescence intensity in MCF-7 cells treated with Apt-Urn-Lip *versus* those treated with Ctrl-Urn-Lip (Table S1†). It is also noticeable that 93.6% of cells incubated with Apt-Urn-Lip for 4 hours showed a fluorescent response, compared to 57.0% for Ctrl-Urn-Lip (Table S1†). When the concentration of Urn-Lip was increased to 500 μM, a similar trend was also observed (Fig. S5†). The results clearly demonstrated the enhanced binding of Apt-Urn-Lip to the MCF-7 cells compared with Ctrl-Urn-Lip, presumably due to the selective affinity between the NCL aptamer and the nucleolin which was overexpressed on the plasma membrane of MCF-7 cells.
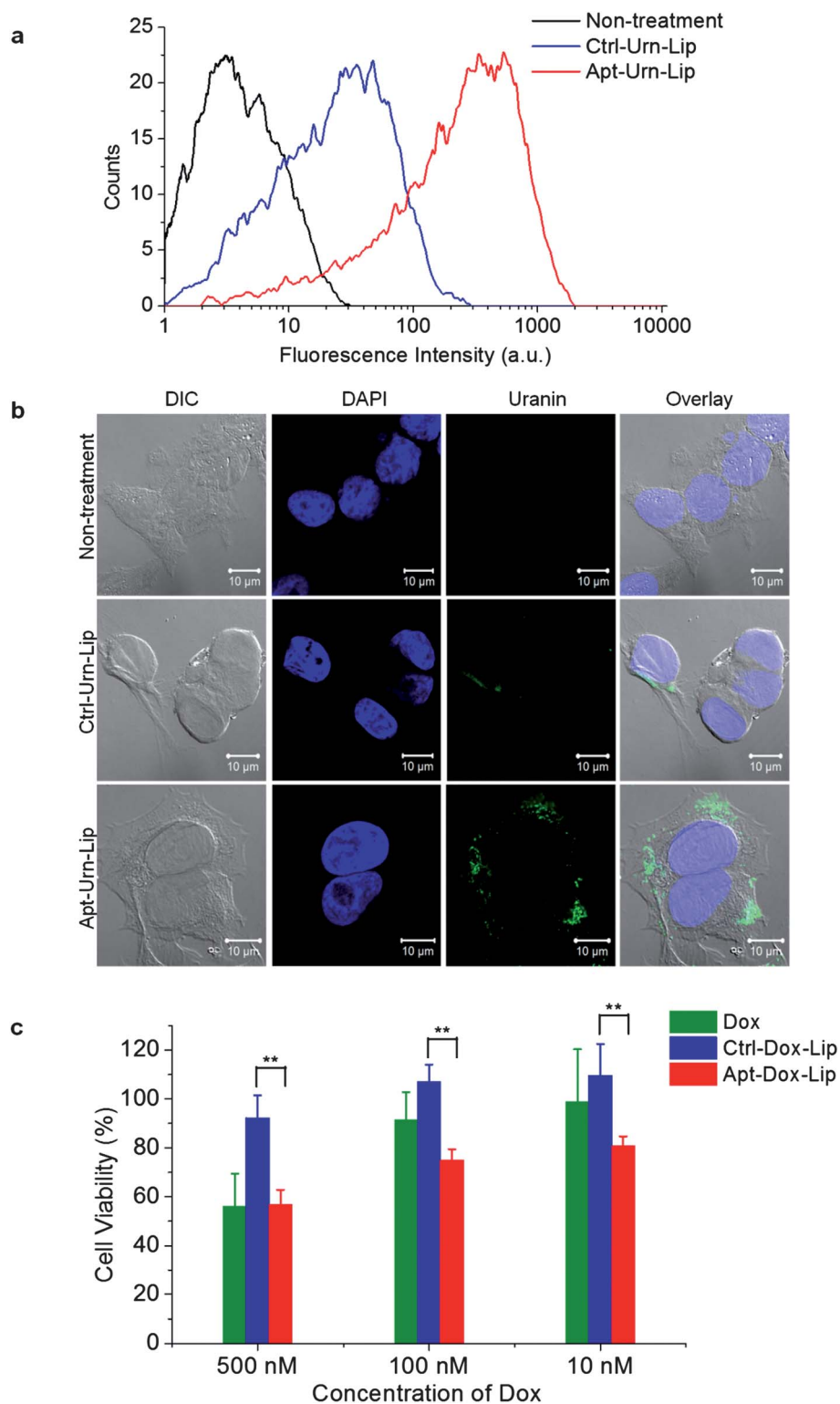
We next investigated whether the increased binding of Apt-Urn-Lip to MCF-7 cells indeed resulted in enhanced cellular uptake of liposomes by MCF-7 cells. Using confocal fluorescence microscopy with fine *z*-axis resolution, we studied the localization of Urn-Lip in the treated cells (Fig. 4b). The nuclei of MCF-7 cells were stained with 4′,6-diamidino-2-phenylindole (DAPI, shown as blue in Fig. 4b), and the liposomes were labeled with uranin (shown as green in Fig. 4b). In order to better demonstrate the specificity between targeted (MCF-7) and non-targeted cells (LNCaP), a higher sample concentration (500 μM lipid equivalent) was used. To avoid saturation of fluorescent signal in MCF-7 cells under such as a high concentration, cells were incubated for a shorter time (2 h). More green fluorescence was observed in the cytoplasm of the MCF-7 cells treated with Apt-Urn-Lip than Ctrl-Urn-Lip, demonstrating that Apt-Urn-Lip was more efficiently internalized by MCF-7 cells. Furthermore, Apt-Urn-Lip was specifically internalized by cells which over-express NCL on the cell membrane, *i.e.* MCF-7 cells (NCL(+)), but not by LNCaP cells (NCL(−)) (Fig. S6†). Together, these results showed that the NCL aptamer-modified liposomes targeted MCF-7 cells selectively and efficiently due to the specific binding of the aptamer to NCL overexpressed on cell membrane.

To evaluate whether the NCL aptamer-functionalized, Dox-containing liposomes can increase the toxicity of the drug to the cancer cells, we further investigated the cytotoxicity of

Fig. 3 (a) Fluorescent spectra of Apt-Urn-Lip sample solution at 1 : 500 dilution in 50% human serum after incubation at 37 °C for different lengths of time. λ_{ex} = 490 nm; λ_{em} = 515 nm. Heat treatment was used to facilitate the rupture of liposomes. (b) Timecourse study of uranin release from liposomes at 37 °C in 50% human serum.

This journal is © The Royal Society of Chemistry 2013

J. Mater. Chem. B, 2013, **1**, 5288–5297 | **5291**

Fig. 4 *In vitro* study of breast cancer cell targeting. (a) Flow cytometry analysis of MCF-7 cells treated with Ctrl-Urn-Lip or Apt-Urn-Lip. MCF-7 cells (200 000 per well) were plated in a 12-well plate. The cells were treated with liposome (50 μM lipids in equivalent) labeled with uranin at 37 °C for 4 h. Each group received liposomes with same total fluorescence intensity. The cells were then washed, trypsinized, and fixed in 4% paraformaldehyde solution for flow cytometry analysis. (b) Confocal microscope images of MCF-7 cells treated with Ctrl-Urn-Lip or Apt-Urn-Lip. MCF-7 cells (250 000 per well) were plated in a 4-well chamber slide and treated with Ctrl-Urn-Lip or Apt-Urn-Lip with same total fluorescence intensity at 37 °C for 4 h. Nuclei were stained by DAPI (blue). Liposomes were labeled with uranin (green). (c) Cytotoxicity study of Ctrl-Dox-Lip and Apt-Dox-Lip samples. MCF-7 cells (3000 per well) were plated in a 96 well plate 24 h before study. MCF-7 cells were treated with free Dox, Ctrl-Dox-Lip or Apt-Dox-Lip at various concentrations of Dox or Dox equivalent for 6 h at 37 °C. The cells were subsequently washed and incubated in media for a total of 72 h before assessing cell viability by MTT assay in each group. **$p < 0.01$, Student *T*-test.

5292 | *J. Mater. Chem. B*, 2013, **1**, 5288–5297

This journal is © The Royal Society of Chemistry 2013

doxorubicin-loaded, PEGylated liposomes, modified either with NCL aptamer (Apt-Dox-Lip) or a control DNA sequence (Ctrl-Dox-Lip). In order to give MCF-7 cells sufficient time to take up enough liposomes or drugs to compare the cytotoxicity after another 3 days, cells were incubated with Dox, Ctrl-Dox-Lip or Apt-Dox-Lip samples for 6 h. The cells were further cultured in fresh medium for a total of 72 h before the assessment of cell viability by MTT assay. The results suggested that Apt-Dox-Lip showed significantly higher cytotoxicity to MCF-7 cells as compared to Ctrl-Dox-Lip ($p < 0.01$). As shown in Fig. 4c, the cell viabilities were $57.0 \pm 6\%$, $75.0 \pm 4\%$, and $80.9 \pm 4\%$ (mean $\pm$ SD) for MCF-7 cells treated with Apt-Dox-Lip at equivalent Dox concentration of 500 nM, 100 nM and 10 nM, respectively. In contrast, the cell viabilities were $92.4 \pm 9\%$, $107.2 \pm 7\%$, and $109.7 \pm 13\%$ for cells treated with Ctrl-Dox-Lip at the same concentrations, respectively. There was no statistical significance when comparing the cytotoxicity of free Dox and Apt-Dox-Lip, suggesting that all the Dox loaded in Apt-Dox-Lip was eventually released and available to the cancer cells. Although the AS1411 aptamer itself has been reported to be cytotoxic towards MCF-7 cells,[40] the amount of aptamer used here was much less than that necessary to cause significant cell death.[41] The cell viability was mainly determined by the amount of Dox delivered into the MCF-7 cells. Therefore, Apt-Dox-Lip can strongly bind to and be internalized by MCF-7 cells, leading to selective delivery of the encapsulated anticancer drug into cells and improved antiproliferative activity in cancer cells *in vitro*.

In vivo antitumor efficacy of aptamer-functionalized liposomes
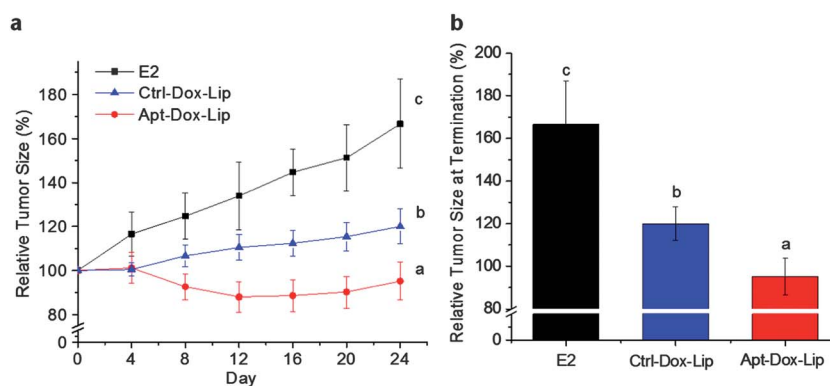
We next examined the efficacy of Apt-Dox-Lip on the inhibition of growth of MCF-7 tumors, which were established by injecting MCF-7 cells subcutaneously into athymic nude mice. Human breast cancer MCF-7 cells are hormone-dependent cells, requiring estrogen to maintain the growth of primary tumors in mice.[42,43] Therefore, the engraftment and growth of MCF-7 tumors was supported by estrogen pellets subcutaneously implanted in the interscapular region of mice prior to cell

injection. Nude mice were treated with Apt-Dox-Lip or Ctrl-Dox-Lip (25 µg Dox equivalent per tumor) every 4 days. Tumors were measured every 4 days, and the tumor growth curves are displayed in Fig. 5a. Tumors in the E2 group maintained a high growth rate in the presence of exogenous estrogen released by the E2 pellets, and the relative average tumor size increased to 166% at the end of the study (Day 24) compared to the tumor size at the start of treatment (Fig. 5b). Analysis of relative tumor size using the PROC MIXED of SAS showed that the Apt-Dox-Lip significantly inhibited MCF-7 tumor growth induced by E2 through the study duration, and was more effective than the Ctrl-Dox-Lip control group ($p = 0.004$, Fig. 5a). At the end of the study, the observed relative tumor size of 95% in the Apt-Dox-Lip group was significantly different from the 120% observed in the Ctrl-Dox-Lip group (Fig. 5b). Furthermore, treatment with Apt-Dox-Lip caused an earlier onset of tumor inhibition on Day 8 when compared with the onset of Day 16 in Ctrl-Dox-Lip (Table S2†). These results strongly suggested that Apt-Dox-Lip inhibited estrogen-induced MCF-7 tumor growth more effectively when compared with Ctrl-Dox-Lip.

To examine the toxicity of Apt-Dox-Lip to mice, the body weights of mice were monitored weekly to assess their overall health. The SAS PROC MIXED analysis of the interaction of time and treatment showed no difference between the E2, Apt-Dox-Lip and Ctrl-Dox-Lip groups (Fig. S7a†), indicating that the overall health of the animals was not affected during the course of the study. The 3 experimental groups also maintained 100% survival rate throughout the study. Daily food intake was measured twice, and no significant differences were found in food intake among the 3 experimental groups in this study (Fig. S7b†).

Tumor penetration study of aptamer-functionalized liposomes

To investigate the possible reasons for the enhanced efficacy of Apt-Dox-Lip in suppressing MCF-7 tumor growth, we compared the tumor penetration behavior of Apt-Dox-Lip and Ctrl-Dox-Lip after they were injected intratumorally into the MCF-7 tumors

Fig. 5 (a) Apt-Dox-Lip inhibited estrogen-induced human breast MCF-7 tumor growth more efficiently when compared to Ctrl-Dox-Lip. Apt-Dox-Lip and Ctrl-Dox-Lip (25 µg doxorubicin equivalent per tumor) were directly injected into tumors every 4 days. The cross sectional area of each tumor was calculated at each time point, and standardized to be expressed as a percentage of the tumor area at the onset of treatment. Data were analyzed using the PROC MIXED of SAS, and curves with different letters indicate significant differences at the level of 0.05. (b) Relative tumor size in each treatment group at the end of the study. Data were analyzed using one-way ANOVA with post hoc Fisher's LSD test. Bars with different letters indicate significant difference at the level of $p < 0.05$.
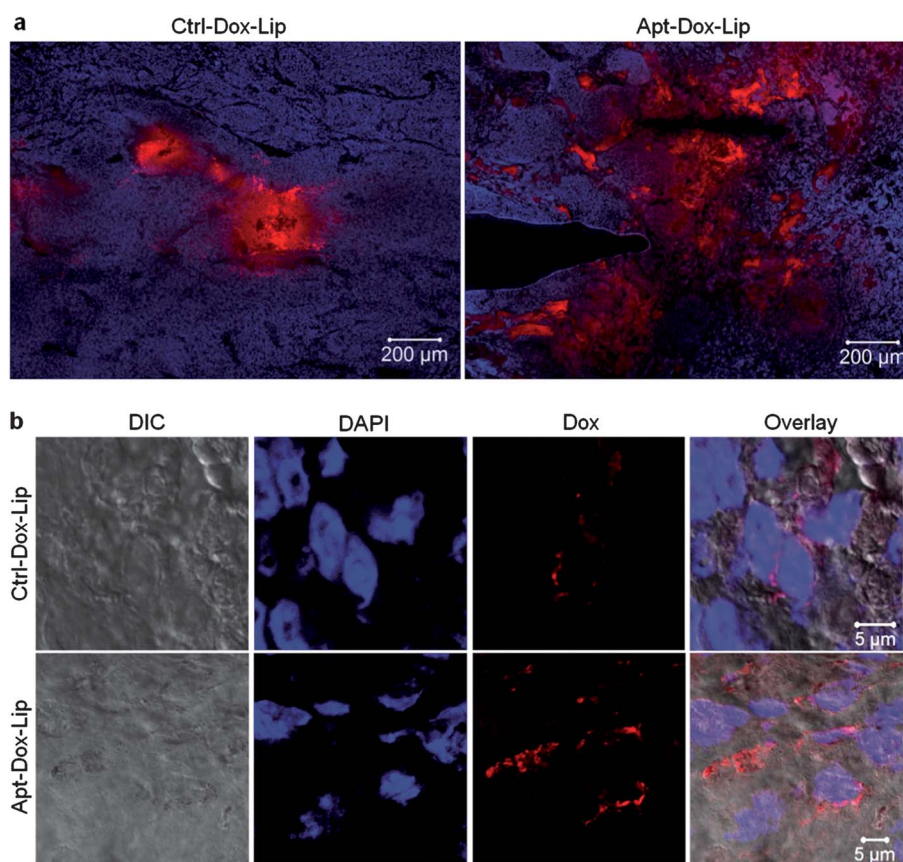
in mice. The tumors were collected 1 h post injection, sectioned and stained with DAPI (Fig. 6a). The fluorescence microscope images of the whole injection area revealed a marked increase of penetration depth into surrounding tumor tissues by Apt-Dox-Lip as compared to Ctrl-Dox-Lip (doxorubicin fluorescence shown in red). The fluorescence intensity plot profile was analyzed by ImageJ, as shown in Fig. S8.† The center of peak correlates to the initial injection site and the half width of the peak is an estimate of the penetration radius from the injection site to the surrounding tissues. Tumor sections treated with Apt-Dox-Lip showed not only overall enhanced fluorescence intensity (y axis of Fig. S8†), but also a larger area with fluorescence (x axis of Fig. S8†). Apt-Dox-Lip penetrated up to ∼1000 μm from the injection site at 1 h post injection while Ctrl-Dox-Lip exhibited much smaller penetration depth (∼500 μm).

The passive diffusion of the liposomes into tumors was also evaluated in an *ex vivo* experiment to compare their penetration in tumor tissues mimicking the situation of a intratumoral injection of liposomes. MCF-7 tumors collected from athymic nude mice were incubated with Apt-Urn-Lip or Ctrl-Urn-Lip in cell medium for 24 h. The tumors were then collected, sectioned, stained with DAPI and imaged *via* confocal microscope. The results shown in Fig. S9† suggest that Apt-Urn-Lip

was taken up more in tumor tissues than Ctrl-Urn-Lip (uranin shown in green fluorescence). Together, these results demonstrated that Apt-Dox-Lip could better penetrate MCF-7 tumor tissue due to the targeting effect of surface bound NCL-Apt, thus facilitating the efficient delivery of anticancer drugs more deeply into tumor tissues than Ctrl-Urn-Lip. This could be one of the reasons that Apt-Urn-Lip showed improved efficacy against MCF-7 tumors.

To further determine whether the liposomes were actually internalized by cancer cells inside tumor tissue or simply stayed in the interstitial space of tumor tissues, the MCF-7 cells in the tumor tissue sections were analyzed with confocal fluorescence microscopy (Fig. 6b). Much more red fluorescence was observed inside MCF-7 cells in the tissue sections from the mice treated with Apt-Dox-Lip than Ctrl-Dox-Lip, suggesting that the targeted liposomes also enhanced cellular internalization *in vivo*. This result agreed well with the observed enhancement in internalization by MCF-7 cells *in vitro* as demonstrated above.

Apt-Dox-Lip is shown to be taken up by MCF-7 cells efficiently, resulting in more efficient delivery of the anticancer drug doxorubicin to cancer cells *in vivo*, thus leading to more efficient killing of cancer cells. These results are comparable with previous reports using anti-HER2 antibody[44] and

Fig. 6 *In vivo* tumor penetration study. (a) Fluorescence microscope images of MCF-7 tumor sections. Athymic nude mice bearing MCF-7 tumor (∼5.0 × 5.0 mm, n = 3) were administered with Ctrl-Dox-Lip or Apt-Dox-Lip by intra-tumor injection. The mice were sacrificed and the tumors were collected 1 h post injection. The tumors were flash frozen in OCT, sectioned (10 μm thickness), and stained with DAPI for nucleus. The tumor sections were analyzed by confocal fluorescence microscopy. (b) Confocal fluorescence microscope images of MCF-7 cells in tumor sections.

5294 | *J. Mater. Chem. B*, 2013, **1**, 5288–5297

This journal is © The Royal Society of Chemistry 2013

transferrin[45] as targeting ligands. Likely, the active targeting ligand on the liposome surface played a role in sub-organ distribution and *in vivo* cellular internalization. Once the liposomes are inside the tumors, the specific binding between Apt-Dox-Lip and nucleolin expressed on MCF-7 cell surface facilitate the enhanced tissue penetration and internalization by cancer cells.

Conclusions

In conclusion, we have demonstrated the successful formulation of doxorubicin-encapsulated, AS1411 aptamer-functionalized liposomes as a drug delivery system that was able to target nucleolin. *In vitro* studies showed the high targeting efficiency of AS1411 aptamer-functionalized liposomes toward MCF-7 cells with overexpressed nucleolin. Enhanced cytotoxicity and antitumor efficacy were observed in MCF-7 cells and in MCF-tumor bearing mice with the use of AS1411 aptamer-functionalized liposomes *versus* control liposomes. Aptamer-functionalized liposomes exhibited enhanced tumor penetration ability, which could account for the improved antitumor efficacy observed *in vivo*. In conjunction with the high stability and excellent biocompatibility of liposomes, the AS1411 aptamer-functionalized liposome demonstrated here shows excellent potential as a new modality for targeted cancer therapy.

Materials and methods

Chemicals and materials

Chemicals and reagents used in this study were obtained from Sigma-Aldrich Inc. (St. Louis, MO) and used as received. HSPC, cholesterol, mPEG2000-DSPE, and extruder were obtained from Avanti Polar Lipids, Inc (Alabaster, AL). Sephadex G-100 medium was purchased from GE Healthcare (Chalfont St. Giles, UK). OliGreen® ssDNA reagent was obtained from Invitrogen (Carlsbad, CA). All oligonucleotides used in this study were purchased from Integrated DNA Technologies Inc. (Coralville, IA) with the following sequences:

NCL-Aptamer (Apt): 5′-GGT GGT GGT GGT TGT GGT GGT GGT GGT TTT TTT TTT TT-Cholesterol-3′.

Random DNA (Ctrl): 5′-GAG AAC CTG AGT CAG TAT TGC GGA GAT TTT TTT TTT TT-Cholesterol-3′.

Formulation of liposomes

DNA-functionalized liposomes containing either uranin (Urn) or doxorubicin (Dox) were formulated from hydrogenated soy phosphatidylcholine (HSPC), cholesterol, and distearoyl phosphatidyl-ethanolamine modified with methoxy poly(ethylene glycol) with a molecular weight (MW) of 2000 Da (mPEG2000-DSPE) (see ESI†).

Determination of DNA concentration, density and conjugation efficiency

The OliGreen® ssDNA reagent (Invitrogen, USA) was utilized to measure the concentration of DNA strands. DNA-modified liposome samples were treated with Triton-X and heated at 80 °C for 20 minutes to rupture liposomes and release DNA strands prior to the staining process. A standard curve was obtained from a series of standard DNA solutions following manufacturer's instructions (see ESI†).

In vitro cellular internalization and cytotoxicity studies

MCF-7 cells were seeded, washed, and incubated with Opti-MEM containing either Apt-Urn-Lip or Ctrl-Urn-Lip (50 μM lipid equivalent) samples. The cells were stained, fixed, and then subsequently imaged on a confocal laser scanning microscope (LSM700, Carl Zeiss, NY). Cells without the addition of Urn-Lip were imaged as control. Both the percentage of the fluorescent cells relative to the total analyzed cells and the fluorescence intensity of the fluorescence-positive cells were assessed.

Fresh medium containing Dox, Ctrl-Dox-Lip, or Apt-Dox-Lip in concentrations ranging from 10 nM to 500 nM of Dox or equivalent Dox was used for cytotoxicity study. Cell viability was determined by the MTT assay (see ESI Section S3†). Standard MTT assay protocols were followed thereafter.[46]

Animals

Female athymic nude mice were purchased from Charles River (Wilmington, MA) and ovariectomized at the age of 21 days by the vendor. After arrival, mice were single-cage housed, with free access to food and water. Artificial light was provided in a 12/12 hour cycle. The AIN-93G semi-purified diet (Dyets, Bethlehem, PA) was selected as it has been established to meet the nutritional requirements of mice.[47] Animals were maintained under animal protocols approved by the Institutional of Animal Care and Use and Committee at the University of Illinois at Urbana-Champaign.

Efficacy study using MCF-7 xenografts

A 1 mg estrogen pellet (1 mg : 19 mg estrogen : cholesterol) was subcutaneously implanted into the intrascapular region on each mouse. Four days after pellet implantation, human breast cancer MCF-7 cells were suspended in Matrigel™ and subcutaneously injected into four sites (2×10^5 cells per site) on the flank of each mouse. Tumors were measured with a caliper every four days, and the tumor cross sectional area was calculated using the formula (length/2) × (width/2) × 3.14.[48] When the average tumor cross sectional area reached 40 mm^2, the animals were normalized by their tumor size and distributed into 3 groups: estrogen (E2) group (animal $n = 4$, tumor $n = 11$), Apt-Dox-Lip group (animal $n = 5$, tumor $n = 21$), Ctrl-Dox-Lip group (animal $n = 6$, tumor $n = 22$), and the treatment was initiated. Apt-Dox-Lip or Ctrl-Dox-Lip (25 μg Dox equivalent) was directly injected into each tumor every 4 days for 24 days. The mice in the estrogen group received the same volume of PBS per tumor. The cross sectional area of each tumor was calculated at each time point, and expressed as a percentage of the tumor area at the onset of treatment (100%), as described previously. Daily food intake was measured twice, the first time 3 weeks post cell injection (measurement 1, M1) and the second time 3

weeks post treatment initiation (M2). Body weight was monitored weekly.

Ex vivo tumor penetration study

Female athymic nude mice bearing MCF-7 tumors were sacrificed to collect the tumors when the average tumor size reached ~4.0 × 4.0 mm. Whole tumors ($n = 3$) were *ex vivo* cultured with Ctrl-Urn-Lip or Apt-Urn-Lip at concentration of 10 μg equivalent uranin per mL in cell medium for 24 h. Tumors without any treatment served as the control. Tumor sections (5 μm) were collected by cryostat, mounted on glass slides, and imaged.

In vivo tumor penetration study

Female athymic nude mice bearing MCF-7 tumors were divided randomly into groups of three ($n = 3$) and were treated when the average tumor size reached 5.0–6.0 mm. Animals in each group received a PBS solution, Ctrl-Dox-Lip, or Apt-Dox-Lip (25 μL, 1 mg doxorubicin equivalent per mL) respectively through intratumoral injection. The animals were euthanized 1 h after administration, and tumor sections (10 μm) were collected by cryostat, mounted on glass slides, and imaged.

Statistics

All statistical data analysis was conducted using either SAS™ 9.2 (SAS Institute Inc., Cary, NC) or OriginPro® 8.5 (OriginLab Corporation, Northampton, MA) program. Data of food intake and tumor size measured on the same time point were analyzed using one-way ANOVA (OriginPro) with *post hoc* Fisher's LSD test. Continuous data of body weight or tumor size over the duration of the study were analyzed using the PROCEDURE MIXED of SAS. $P < 0.05$ was considered significantly different between treatment groups.

Acknowledgements

Notes and references

1 J. Cheng, B. A. Teply, I. Sherifi, J. Sung, G. Luther, F. X. Gu, E. Levy-Nissenbaum, A. F. Radovic-Moreno, R. Langer and O. C. Farokhzad, *Biomaterials*, 2007, **28**, 869–876.

2 D. Peer, J. M. Karp, S. Hong, O. C. Farokhzad, R. Margalit and R. Langer, *Nat. Nanotechnol.*, 2007, **2**, 751–760.

3 S. Aryal, C. M. J. Hu and L. F. Zhang, *ACS Nano*, 2010, **4**, 251–258.

4 C. Kim, B. P. Shah, P. Subramaniam and K. B. Lee, *Mol. Pharmaceutics*, 2011, **8**, 1955–1961.

5 C. L. Zhu, L. B. Liu, Q. Yang, F. T. Lv and S. Wang, *Chem. Rev.*, 2012, **112**, 4687–4735.

6 S. C. Alley, N. M. Okeley and P. D. Senter, *Curr. Opin. Chem. Biol.*, 2010, **14**, 529–537.

7 Y. M. Yang, F. Liu, X. G. Liu and B. G. Xing, *Nanoscale*, 2013, **5**, 231–238.

8 J. C. Reubi, *Endocr. Rev.*, 2003, **24**, 389–427.

9 D. Schrama, R. A. Reisfeld and J. C. Becker, *Nat. Rev. Drug Discovery*, 2006, **5**, 147–159.

10 J. M. Zhang, P. L. Yang and N. S. Gray, *Nat. Rev. Cancer*, 2009, **9**, 28–39.

11 A. K. Gupta, R. R. Naregalkar, V. D. Vaidya and M. Gupta, *Nanomedicine*, 2007, **2**, 23–39.

12 T. Lammers, S. Aime, W. E. Hennink, G. Storm and F. Kiessling, *Acc. Chem. Res.*, 2011, **44**, 1029–1038.

13 P. Sapra and T. M. Allen, *Prog. Lipid Res.*, 2003, **42**, 439–462.

14 A. D. Keefe, S. Pai and A. Ellington, *Nat. Rev. Drug Discovery*, 2010, **9**, 537–550.

15 D. Shangguan, Y. Li, Z. W. Tang, Z. H. C. Cao, H. W. Chen, P. Mallikaratchy, K. Sefah, C. Y. J. Yang and W. H. Tan, *Proc. Natl. Acad. Sci. U. S. A.*, 2006, **103**, 11838–11843.

16 O. C. Farokhzad, J. Cheng, B. A. Teply, I. Sherifi, S. Jon, P. W. Kantoff, J. P. Richie and R. Langer, *Proc. Natl. Acad. Sci. U. S. A.*, 2006, **103**, 6315.

17 J. W. Guo, X. L. Gao, L. N. Su, H. M. Xia, G. Z. Gu, Z. Q. Pang, X. G. Jiang, L. Yao, J. Chen and H. Z. Chen, *Biomaterials*, 2011, **32**, 8010–8020.

18 W. A. Zhao, M. M. Ali, M. A. Brook and Y. F. Li, *Angew. Chem., Int. Ed.*, 2008, **47**, 6330–6337.

19 J. W. Liu, Z. H. Cao and Y. Lu, *Chem. Rev.*, 2009, **109**, 1948–1998.

20 E. J. Cho, J. W. Lee and A. D. Ellington, *Annu. Rev. Anal. Chem.*, 2009, **2**, 241–264.

21 D. Li, S. P. Song and C. H. Fan, *Acc. Chem. Res.*, 2010, **43**, 631–641.

22 S. S. Oh, K. Plakos, X. H. Lou, Y. Xiao and H. T. Soh, *Proc. Natl. Acad. Sci. U. S. A.*, 2010, **107**, 14053–14058.

23 P. Ray and R. R. White, *Pharmaceuticals*, 2010, **3**, 1761–1778.

24 N. L. Rosi and C. A. Mirkin, *Chem. Rev.*, 2005, **105**, 1547–1562.

25 N. Dave and J. W. Liu, *Adv. Mater.*, 2011, **23**, 3182–3186.

26 Z. H. Cao, R. Tong, A. Mishra, W. C. Xu, G. C. L. Wong, J. J. Cheng and Y. Lu, *Angew. Chem., Int. Ed.*, 2009, **48**, 6494–6498.

27 Y. Kaneda, *Adv. Drug Delivery Rev.*, 2000, **43**, 197–205.

28 J. Schafer, S. Hobel, U. Bakowsky and A. Aigner, *Biomaterials*, 2010, **31**, 6892–6900.

29 H. Maeda, J. Wu, T. Sawa, Y. Matsumura and K. Hori, *J. Controlled Release*, 2000, **65**, 271–284.

30 M. Derenzini, V. Sirri, D. Trere and R. L. Ochs, *Lab. Invest.*, 1995, **73**, 497–502.

31 V. Dapic, V. Abdomerovic, R. Marrington, J. Peberdy, A. Rodger, J. O. Trent and P. J. Bates, *Nucleic Acids Res.*, 2003, **31**, 2097–2107.

32 Y. Otake, S. Soundararajan, T. K. Sengupta, E. A. Kio, J. C. Smith, M. Pineda-Roman, R. K. Stuart, E. K. Spicer and D. J. Fernandes, *Blood*, 2007, **109**, 3069–3075.

33 S. Soundararajan, W. W. Chen, E. K. Spicer, N. Courtenay-Luck and D. J. Fernandes, *Cancer Res.*, 2008, **68**, 2358–2365.

34 P. J. Bates, D. A. Laber, D. M. Miller, S. D. Thomas and J. O. Trent, *Exp. Mol. Pathol.*, 2009, **86**, 151–164.

35 C. R. Ireson and L. R. Kelland, *Mol. Cancer Ther.*, 2006, **5**, 2957–2962.

36 J. W. Park, K. L. Hong, D. B. Kirpotin, G. Colbern, R. Shalaby, J. Baselga, Y. Shao, U. B. Nielsen, J. D. Marks, D. Moore, D. Papahadjopoulos and C. C. Benz, *Clin. Cancer Res.*, 2002, **8**, 1172–1181.

37 Y. Barenholz, *J. Controlled Release*, 2012, **160**, 117–134.

38 M. C. Woodle and D. D. Lasic, *Biochim. Biophys. Acta*, 1992, **1113**, 171–199.

39 D. C. Drummond, O. Meyer, K. L. Hong, D. B. Kirpotin and D. Papahadjopoulos, *Pharmacol. Rev.*, 1999, **51**, 691–743.

40 P. J. Bates, J. B. Kahlon, S. D. Thomas, J. O. Trent and D. M. Miller, *J. Biol. Chem.*, 1999, **274**, 26369–26377.

41 V. Dapic, P. J. Bates, J. O. Trent, A. Rodger, S. D. Thomas and D. M. Miller, *Biochemistry*, 2002, **41**, 3676–3685.

42 C. K. Osborne, K. Hobbs and G. M. Clark, *Cancer Res.*, 1985, **45**, 584–590.

43 P. S. Low, W. A. Henne and D. D. Doorneweerd, *Acc. Chem. Res.*, 2008, **41**, 120–129.

44 D. B. Kirpotin, D. C. Drummond, Y. Shao, M. R. Shalaby, K. L. Hong, U. B. Nielsen, J. D. Marks, C. C. Benz and J. W. Park, *Cancer Res.*, 2006, **66**, 6732–6740.

45 C. H. J. Choi, C. A. Alabi, P. Webster and M. E. Davis, *Proc. Natl. Acad. Sci. U. S. A.*, 2010, **107**, 1235–1240.

46 I. Martin-Kleiner, I. Svoboda-Beusan and J. Gabrilovac, *Immunopharmacol. Immunotoxicol.*, 2006, **28**, 411–420.

47 P. G. Reeves, F. H. Nielsen and G. C. Fahey, *J. Nutr.*, 1993, **123**, 1939–1951.

48 Y. H. Ju, D. R. Doerge, K. F. Allred, C. D. Allred and W. G. Helferich, *Cancer Res.*, 2002, **62**, 2474–2477.